8th Int. Symp. "Nanostructures: Physics and Technology"
St Petersburg, Russia, June 19–23, 2000

Recent results in quantum cascade lasers and applications

Claire Gmachl, Federico Capasso, Alessandro Tredicucci, Rüdeger Köhler, Albert L. Hutchinson, Deborah L. Sivco, James N. Baillargeon and Alfred Y. Cho
Bell Laboratories, Lucent Technologies,
600 Mountain Avenue, Murray Hill, NJ 07974, USA

Abstract. Recent advances in quantum cascade (QC) lasers include widely tunable single-mode distributed feedback (DFB) lasers with high optical power at $\lambda \approx 4.6\,\mu$m, and single-mode DFB lasers at $\lambda \approx 16\,\mu$m based on new surface plasmon waveguides with dual-metal gratings. Single-mode and tunable QC-DFB lasers have successfully been used in many collaborations for various trace-gas sensing applications. Examples are the detection of stratospheric methane and nitrous oxide, the sub-ppbv detection of ammonia by cavity ring down spectroscopy, methane concentration and isotopic composition measurements, and the detection of complex molecules in open air by direct absorption spectroscopy. The versatility of band structure engineering enabled the design and realization of QC-lasers, which operate under both, positive and negative polarity displaying distinct characteristics in each polarity if an asymmetric structure is employed.

Introduction

In the mid-infrared wavelength range only few lasers are established as high power and continuously tunable, narrow linewidth light sources for high-resolution gas sensing applications. The recent development of quantum cascade (QC) and single-mode QC distributed feedback (DFB) lasers [1, 2], however, offers a new and promising alternative. The possibility of achieving amplification from electronic transitions within one band of a semiconductor heterostructure was first postulated by R. F. Kazarinov and R. A. Suris [3]. Semiconductor QC-lasers are consequently based on such electronic transitions between quantized conduction band states of a multiple quantum well structure. They are designed through band-structure engineering and grown by molecular beam epitaxy (MBE).

1. Quantum cascade distributed feedback lasers

Here, we first present QC-DFB lasers designed and fabricated for various trace gas sensing applications. Figure 1 shows an overview of the continuous single-mode tuning ranges of selected lasers operated in pulsed mode. Incorporation of a strong Bragg-grating into the waveguide of the QC-DFB laser leads to very large tuning ranges of approximately 100 and 150 nm for 5 μm and 10 μm wavelength lasers, respectively. In the following we will discuss as two examples the shortest (4.6 μm) [4] and longest (16.2 μm) [5] QC-DFB lasers in more detail.

While the early work on QC-DFB lasers was motivated by feasibility proofs, our later work on QC-DFB lasers is strongly guided by applications. Trace-gases such as CO or CO_2 and their isotopes are of great environmental and medical importance; however, the short wavelengths of their fundamental rotational-vibrational transitions between 4 and 5 μm wavelength are largely out of reach of conventional QC-lasers. Here, we present short-wavelength single-mode and tunable QC-DFB lasers using strained InGaAs/AlInAs

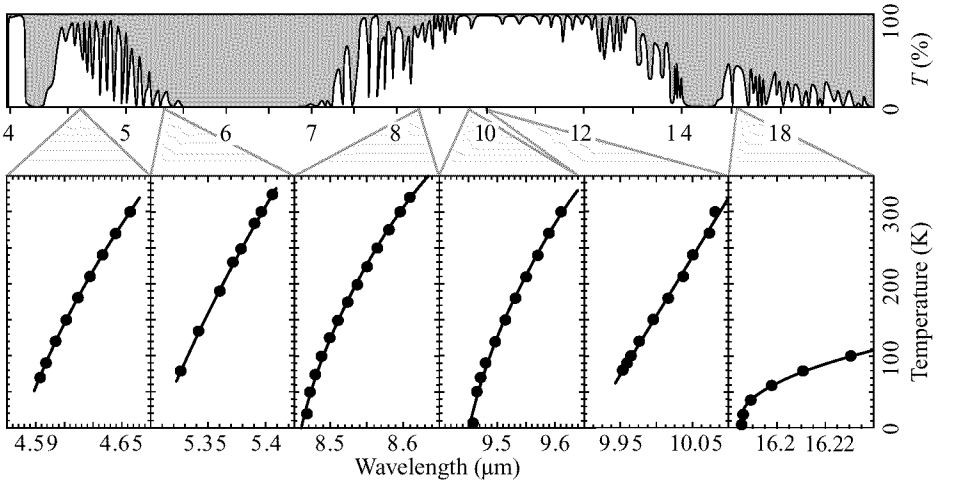

Fig. 1. Top: The area under the curve shows the transmission of the atmosphere at sea level. Bottom: Single-mode tuning ranges of selected QC-DFB lasers operated in pulsed mode.

material in the active region [6]. Strained layers increase the band-offset between the quantum wells and barriers ($In_{0.62}Ga_{0.38}As$ wells and $Al_{0.6}In_{0.4}As$ barriers result in a band-offset of ~0.725 eV), thus allowing good quantum confinement also for the upper laser state and a concomitant good device performance. The lasers emit in the wavelength range of 4.6–4.7 μm, where they overlap with one major branch of the CO rotational-vibrational absorption spectrum. These new devices have unprecedented pulsed peak output power levels of ~100 mW at room temperature and ~150 mW in continuous wave at 80 K. The design of the active region is of the so-called 'three well vertical' type with InGaAs and AlInAs lattice-matched to InP. This operating principle is for the $\lambda = 4.6\,\mu$m laser in more detail discussed in reference [4] and references therein. These lasers contained a waveguide core comprised of $N = 26$ active region stages alternated with electron injectors. A high number of stages is essential for high optical output power and slope efficiency. The waveguide core further contained low doped InGaAs layers below and above the active regions/injectors stack. The lower waveguide cladding is formed by the low-doped InP-substrate. An inner low-doped AlInAs layer and an outer highly doped AlInAs layer, designed for plasmon-enhanced confinement [7], form the upper waveguide cladding. The first-order Bragg-grating of appropriate period ($\Lambda = 730-750$ nm) is transferred into this last layer using optical contact lithography and wet chemical etching to a depth that essentially removes the plasmon confining layer in the grating grooves. The grating is subsequently covered with top contact metallization of 30 nm Ti / 300 nm Au, resulting in a complex coupling scheme of the DFB laser. The coupling coefficient amounts to $|\kappa| \sim 16\,\mathrm{cm}^{-1}$, and is dominated by the modulation of the effective refractive index. Reliable single-mode output is achieved from 90 to 300 K. The tuning with heat sink temperature is well approximated by a quadratic function and covers ~65 nm with the tuning coefficient increasing linearly from 0.2 nm/K to 0.33 nm/K. In single-mode operation we achieve a side mode suppression ratio of ~30 dB independent of the current level. Peak power levels of 100 mW and a slope efficiency of 180 mW/A at room temperature and ~400 mW/A at low temperatures are achieved.

QC-DFB lasers as the ones described above rely on dielectric waveguides and a Bragg-

grating that was etched into one or more layers of that dielectric waveguide. This approach is very successful for QC-DFB lasers with wavelengths $\lambda \sim 11\ \mu$m. It becomes, however, impractical for very long ($\lambda \sim 17\ \mu$m) wavelength lasers as thick waveguides and very deep gratings would be needed. As a solution to this problem another type of optical confinement—at the interface between two different homogenous materials—can be used. These 'surface plasmon' modes, characterized by an exponentially decaying intensity in the two directions normal to the interface, exist provided the dielectric constants of the two materials have real parts of opposite sign. Negative dielectric constants are encountered e.g. in metals. For wavelengths approaching the far-infrared ($\lambda \geq 15\ \mu$m), the penetration depth into the metal is greatly reduced, yielding low optical losses and a concomitant large transverse optical-mode confinement factor.

Here we present a high performance surface plasmon laser operating at ($\lambda \sim 16\ \mu$m. In order to extend the concept of DFB to such surface plasmon lasers, a two-metal grating deposited on top of the semiconductor was used to produce a strong index contrast due to the large spatial modulation of the skin depth.

Our device employs QC active material with a variable period superlattice active region of the type described in reference [8]. Samples comprising 35 to 40 superlattice/injector stages were grown by MBE. The growth of the active material was preceded by a $\sim$1 μm thick InGaAs layer and followed by thin, highly doped contact layers. The wafers were processed into deep etched ridges. A very wide portion of the top of the ridges was left open for the deposition of the metallic surface-plasmon carrying layer. Deposition of 10 nm of titanium before the final gold layer already results in a relative change of the refractive index of $\sim 1.8 \times 10^{-3}$, compared to pure gold, and of the losses of $\sim 1.5 \times 10^{-2}$. To spatially modulate this variation along the ridge, we fabricated a first-order Bragg grating of an alternate sequence of Ti/Au and pure Au stripes along the surface plasmon propagation. For a grating period $\Lambda = 2.05\ \mu$m, we compute a complex coupling coefficient for the DFB mode $|\kappa| = 6.9\,\mathrm{cm}^{-1}$ which is dominated by the real part. Figure 1 also shows the single mode tuning range of this laser. The change of the modal refractive index with temperature can again be used as an effective way to tune the laser frequency; a linear tuning coefficient is found at the highest temperatures with a value of 1 nm/K.

2. Trace gas sensing application using QC-DFB lasers

Single-mode and tunable QC-DFB lasers at various wavelengths from 5.2 to 8.6 μm are presently used in collaborations with expert spectroscopists for various trace gas sensing applications, several of which are referenced below. To achieve a narrow linewidth, the lasers are operated in continuous wave. The tuning of the single-mode output is accomplished by varying the current through the device and by Joule's heating. C. Webster and coworkers [9] at the Jet Propulsion Laboratory, conducted measurements of the concentration of CH_4 and N_2O in Earth's atmosphere from ground level to the stratosphere using a 7.95 μm QC-laser on board a high-altitude air-plane. B. Paldus and coworkers [10] at Informed Diagnostics have also demonstrated sub-ppbv (NH_3) sensitivity measurements using cavity ring down spectroscopy. A. A. Kosterev *et al.* [11] at Rice University, TX, reported on measurements of the concentration of $^{12}CH_4$, its natural isotopes $^{13}CH_4$ and $^{12}CH_3D$, H_2O, N_2O, and C_2H_5OH diluted in standard air using a direct absorption technique around 7.95 μm wavelength. R. Williams *et al.* [12] at PNNL in collaboration with M. Taubman and J. Hall at JILA, CO, measured the intrinsic linewidth of several of our QC-DFB lasers around 8 μm wavelength as $\sim$1 MHz. The laser could furthermore be electronically stabilized to a linewidth <20 kHz.

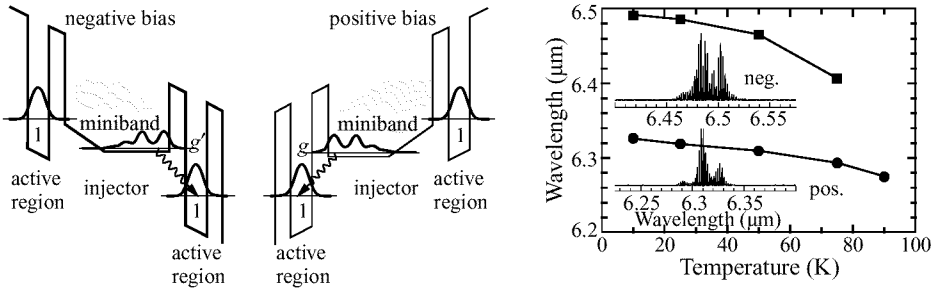

Fig. 2. Left: Schematic band structure of the bi-directional laser under the two bias conditions. Wavy arrows indicate the laser transitions. Right: Fabry–Perot spectra and tuning curves of the asymmetric bi-directional laser under the two different bias-conditions.

3. Bi-directional quantum cascade laser

Band-structure engineering of unipolar structures is a very powerful tool for the design and fabrication of devices with particular characteristics. We recently demonstrated a bi-directional QC-laser with emission wavelength dependent on bias-polarity, $\lambda^- \approx 6.5\,\mu$m and $\lambda^+ \approx 6.35\,\mu$m [13]. This is a new concept for the generation of two wavelengths from a single laser device. In fact, a single device appears as being made of two different laser materials according to the two bias-polarities. Few constraints are posed upon the two wavelengths, which can even be arbitrarily close. We demonstrated this by another bi-directional laser with $\lambda^- \approx \lambda^+ \approx 6.75\,\mu$m. The wavelengths are excited separated in time, which simplifies multiple-wavelength detection schemes, such as differential LIDAR (light detection and ranging).

Figure 2, left, shows the principle of operation of the bi-directional QC-laser. The devices used a so-called 'diagonal' laser transition [14], where the upper laser state is the ground state of the injector region and the lower laser state is residing in a single 'active region' quantum well, bridging successive injectors together. To obtain an asymmetric bi-directional laser, the injector is designed asymmetric by locally modifying quantum well and barrier thickness, while for a symmetric laser the injector region is designed entirely symmetric. The lasers displayed a good threshold current density of $\sim$3 kAcm^{-2}, and peak powers of $\sim$ 300 mW at cryogenic temperatures. Maximum pulsed operating temperature at present is $\sim$150 K. As expected, for the symmetric structure, the emission wavelength was independent of bias polarity, $\lambda^- \approx \lambda^+ \approx 6.75\,\mu$m. Figure 2, right, shows the emission spectra of a device from the asymmetric, bi-directional QC-laser. The laser emits at the different wavelengths $\lambda^- \approx 6.5\,\mu$m and $\lambda^+ \approx 6.35\,\mu$m, and displays the Fabry–Perot spectra typical for ridge waveguide structures. The lasers produce a peak output power of $\geq$100 mW at cryogenic temperatures independent of the bias polarity.

Acknowledgement

This material is based upon work supported in part by DARPA/US Army Research Office under Contract No DAAG55-98-C-0050. R. K. acknowledges support by Studienstiftung des Deutschen Volkes, Deutschland.

References

[1] F. Capasso, C. Gmachl, D. L. Sivco and A. Y. Cho, *Physics World* **12**, 27 (June 1999) and references therein.

[2] J. Faist, C. Gmachl, F. Capasso, C. Sirtori, D. L. Sivco, J. N. Baillargeon, A. L. Hutchinson and A. Y. Cho, *Appl. Phys. Lett.* **70**, 2670 (1997).

[3] R. F. Kazarinov and R. A. Suris, *Fiz. Tekh. Poluprov.* **5**, 797 (1971) [Sov. Phys.- Semicond. **5**, 707 (1971)]

[4] R. Köhler, C. Gmachl, F. Capasso, A. Tredicucci, D. L. Sivco, S. N. G. Chu and A. Y. Cho, *Appl. Phys. Lett.* **76**, 1092 (2000).

[5] A. Tredicucci, C. Gmachl, F. Capasso, A. L. Hutchinson, D. L. Sivco and A. Y. Cho, *Appl. Phys. Lett.* (2000) (accepted for publication).

[6] J. Faist, F. Capasso, D. L. Sivco, A. L. Hutchinson, S. N. G. Chu and A. Y. Cho, *Appl. Phys. Lett.* **72**, 680 (1998).

[7] C. Sirtori, J. Faist, F. Capasso, D. L. Sivco, A. L. Hutchinson and A. Y. Cho, *Appl. Phys. Lett.* **66**, 3242 (1995).

[8] A. Tredicucci, C. Gmachl, F. Capasso, D. L. Sivco, A. L. Hutchinson and A. Y. Cho, *Appl. Phys. Lett.* **74**, 638 (1999).

[9] C. R. Webster, G. J. Flesch, D. C. Scott, J. Swanson, R. D. May, W. S. Woodward, C. Gmachl, F. Capasso, D. L. Sivco, J. N. Baillargeon, A. L. Hutchinson and A. Y. Cho, *Appl. Opt.* (2000) (submitted).

[10] B. A. Paldus, C. C. Harb, T. G. Spence, R. N. Zare, C. Gmachl, F. Capasso, D. L. Sivco, J. N. Baillargeon, A. L. Hutchinson and A. Y. Cho, *Opt. Lett.* (2000) (accepted for publication).

[11] A. A. Kosterev, R. F. Curl, F. K. Tittel, C. Gmachl, F. Capasso, D. L. Sivco, J. N. Baillargeon, A. L. Hutchinson and A. Y. Cho, *Appl. Opt.* (2000) (submitted).

[12] R. M. Williams, J. F. Kelly, J. S. Hartman, S. W. Sharpe, M. S. Taubman, J. L. Hall, F. Capasso, C. Gmachl, D. L. Sivco, J. N. Baillargeon and A. Y. Cho, *Opt. Lett.* **24**, 1844 (1999).

[13] C. Gmachl, A. Tredicucci, D. L. Sivco, A. L. Hutchinson, F. Capasso and A. Y. Cho, *Science* **286**, 749 (1999) and references therein.

[14] J. Faist, F. Capasso, C. Sirtori, D. L. Sivco, A. L. Hutchinson and A. Y. Cho, *Nature* **387**, 777 (1997).